Non-linear magnetic perturbations during edge localized modes in TCV dominated by low n mode components

RP Wenninger[1], H Reimerdes[2], O Sauter[2], H Zohm[3]

[1]Universitätssternwarte der Ludwig-Maximilians-Universität, München, Germany
[2]Ecole Poytechnique Fédérale Lausanne (EPFL), CRPP, Euratom Association, Lausanne, Switzerland
[3]Max-Planck-Institut für Plasmaphysik, EURATOM Association, Garching, Germany

E-mail: ronald.wenninger@ipp.mpg.de

Abstract. Edge localized modes (ELMs) are instabilities in the edge of tokamak plasmas in the high confinement regime (H-mode). Despite beneficial aspects of ELMs, in a future device the size of the energy loss per ELM must be controlled, in order to avoid intolerable divertor power flux densities. To proceed in understanding how the ELM size is determined and how ELM mitigation methods work it is necessary to characterize the non-linear evolution of ELMs.

This publication presents a detailed analysis of the toroidal structure of dominant magnetic perturbations during type I ELMs in TCV. These signatures of the instability can be observed most intensely in close temporal vicinity to the onset of enhanced D_α-radiation. In particular it is shown that dominant magnetic perturbations already have a rigid toroidal mode structure when they are detected with magnetic probes. This indicates that perturbations associated with this type of ELMs at TCV can not be observed in their linear phase. Furthermore it is demonstrated that the toroidal structure of dominant magnetic perturbations is most often dominated by the $n = 1$ component. This is in clear contrast to typical results of linear stability calculations, leading to the hypothesis that the dominant toroidal mode number from the linear to the non-linear phase has a transition from intermediate to low values. In general, the reported results show that non-linear coupling leads to a significant modification of the mode structure.

1. Introduction

Edge localized modes (ELMs) are instabilities in the edge of tokamak plasmas in the high confinement regime (H-mode). Without them the edge particle transport in ordinary H-mode plasmas is too low to establish stationary plasma profiles. However in a future device large unmitigated ELMs are believed to cause divertor power flux densities far in excess of tolerable material limits. Hence the size of energy loss per ELM must be limited.

The most cited model to describe the instability linked to ELMs is the peeling-ballooning-model [1]. This is a linear MHD model of an instability that is driven by both pressure gradient and edge current density. However it is recognized that quantitative prediction of the ELM size requires non-linear studies [2]. Hence, to proceed in understanding the physics of ELMs and in particular how the ELM size is determined it is necessary to characterize the non-linear evolution of this instability. This publication presents an analysis of the toroidal structure of magnetic perturbations during type I ELMs in TCV. In particular there is evidence that the perturbation is already in the non-linear phase, as soon as it can be detected with magnetic probes. Furthermore it is demonstrated that the toroidal structure of this perturbation is most often dominated by the $n = 1$ component, which is in contrast to typical results of linear stability calculations.

In section 2 the investigated discharges and the main employed diagnostic systems are introduced. Section 3 describes the experimentally obtained data and the results from its analysis. Here the main focus is on dominant magnetic perturbations, which appear in close temporal vicinity to the onset of enhanced D_α-radiation. Next to the analysis of the timing, the dynamics and the propagation of dominant magnetic perturbations their toroidal structure and its evolution is presented as key results. The last section summarizes and discusses the results.

2. Experimental arrangements

2.1. Investigated discharges

The operational space of the TCV tokamak [3] includes diverted H-mode plasmas with a wide range of plasma shapes. The analysis is performed for a set of similar discharges (42062, 43015, 43062, 42547) in a diverted lower single null configuration as illustrated in figure 1. In this publication the results are presented for discharge 42062 [4] as a representative. Key parameters of discharge 42062 are: Plasma current 300kA, magnetic field on magnetic axis 1.43T, safety factor at 95% poloidal flux 2.3, central (pedestal top) electron density $5 \times 10^{19}\mathrm{m}^{-3}(3.8 \times 10^{19}\mathrm{m}^{-3})$, central (pedestal top) electron temperature 2.5keV (0.5keV). The discharge is heated with 135kW ohmic power, 900kW ECRH power (X3) launched from the top of the vacuum vessel and 520kW ECRH power (X2) launched from the low field side in the X-point vicinity.

In a similar discharge (42547) an increase in X2 input power leads to an increase in ELM frequency, documenting the type I character of these ELMs [4]. Therefore it is assumed that the ELMs in 42062 are also of type I. In the following 33 ELMs appearing in discharge 42062 between 0.6s and 0.8s are investigated. They are identified by the time derivative of the D_α-signal exceeding a certain threshold value.

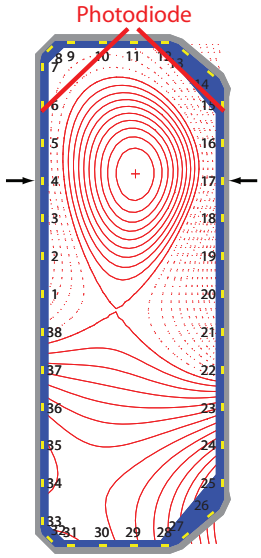

Figure 1. Poloidal cross section of TCV including vacuum vessel (gray), tile aperture (blue), positions of magnetic probes of the poloidal array (yellow) and contours of the poloidal flux (red) for discharge 42062 at 0.7s. The limits of the wide angle view of the optics connected to the photo diode is indicated by two lines. The horizontal arrows indicate the position of the upper toroidal probe sets.

2.2. Key diagnostic systems

TCV is equipped with an extensive set of magnetic probes [5], which are mounted between the wall and graphite protection tiles inside the vacuum vessel. The probes measure the component of the time derivative of the magnetic field, which is tangential to this wall in the poloidal plane. The transfer functions of the probes and also all elements of the amplifying chain have been well characterized and regarded up to approximately 100kHz by a frequency dependent calibration. 12-bit ADCs are used. For the investigated discharge 42062 the sampling rate has been set to 250kHz.

There are toroidal arrays of magnetic probes in three vertical positions consisting of 16 (8) equidistant probes on the outboard side (inboard side). For the analysis of discharge 42062 the upper toroidal probe sets with positions corresponding to probe numbers 17 (outboard) and 4 (inboard) in figure 1 have been used. In this area the vertical measurement direction is in good agreement with the poloidal direction ($\boldsymbol{e}_{\mathrm{pol}} = \frac{\nabla\psi\times\boldsymbol{e}_\phi}{|\nabla\psi\times\boldsymbol{e}_\phi|}$). In the remainder of this publication measured magnetic field into this direction is referred to as B.

D_α-radiation is measured by a photo diode. It is connected to wide angle optics with a view from the top of TCV as indicated in figure 1. Hence the collected light can originate from the main plasma, the outer and inner wall and the divertor region. The signal is sampled with a rate of 50kHz.

3. Magnetic perturbations during ELMs

Perturbations of the poloidal and radial magnetic field during ELMs significantly exceeding the inter-ELM level are regularly observed in tokamak H-mode discharges [6, 7, 8, 9]. Figure 2(a) illustrates a set of subsequent ELMs in discharge 42062. In addition to background fluctuations on the inter-ELM level, during the ELM for periods of up to 0.15ms *dominant magnetic perturbations* are usually observed. These consist of a low number of *dominant magnetic excursions* (figure 2(b)).

Besides ELMs, various other H-mode edge instabilities have been reported to show a comparable characteristic signature recorded by magnetic probes. Some magnetic probes signatures of the edge snake [10], the palm tree mode [11] and the outer mode [12] diverge from a sine. They may rather be characterized by phases of constant signal, periodically interrupted by sets of a low number of dominant excursions lasting in total 0.1ms or less comparable to the ones in figure 2 (b).

To investigate the timing of dominant magnetic excursions, for the probes of the upper outer toroidal array the times $t_{\min}$ and $t_{\max}$ are evaluated, which correspond to the maximum or minimum value of the time derivative of the poloidal magnetic field during the investigated ELM. All 33 ELMs detected in discharge 42062 between 0.6s and 0.8s are considered. As reference time the time $t_{\mathrm{D}\alpha,\mathrm{ons}}$ has been used, at which the ELM associated increase of the D_α-signal exceeds 5% of its peak value. Averaging over toroidal positions and the ELM set gives $t_{\min} = t_{\mathrm{D}\alpha,\mathrm{ons}} - 0.04\mathrm{ms}$ and $t_{\max} = t_{\mathrm{D}\alpha,\mathrm{ons}} - 0.03\mathrm{ms}$. This is about 0.1ms later than in the ASDEX Upgrade case [13], where as reference time the onset of activity (current and radiation) in the divertor has been used. The D_α-signal analyzed in the TCV case originates from both divertor and main chamber (subsection 2.2). This explains the timing difference with respect to the ASDEX Upgrade case.

3.1. Peak and dip trajectories of dominant magnetic excursions

During type I ELMs in TCV the time derivative of the magnetic field measured by magnetic probes exhibits peak values clearly above the inter-ELM level. Figure 3 displays the time derivative of the poloidal magnetic field dB/dt and the variation in the magnetic field δB relative to a time just before the ELM for the outboard side and the inboard side. The slow evolution of δB during the displayed time interval is towards higher (lower) values on the outboard side (inboard side). This is consistent with a movement of the plasma column radially inward due to the ELM related drop in β associated. This rise (fall) in δB is not happening in all toroidal positions at the same time but with a maximum relative time offset of 0.1ms. It is remarkable that the toroidal range, where a given level of δB is reached earlier (later) agrees well on the outboard side and inboard side.

On the plot displaying δB on the outboard side (figure 3(c)) during the last 0.1ms before $t_{\mathrm{D}\alpha,\mathrm{ons}}$ another feature representing relatively high values of δB propagating towards higher toroidal angles can be identified. This feature, which on single channels is well isolated in time (i.e. a single dominant magnetic excursion), constitutes the

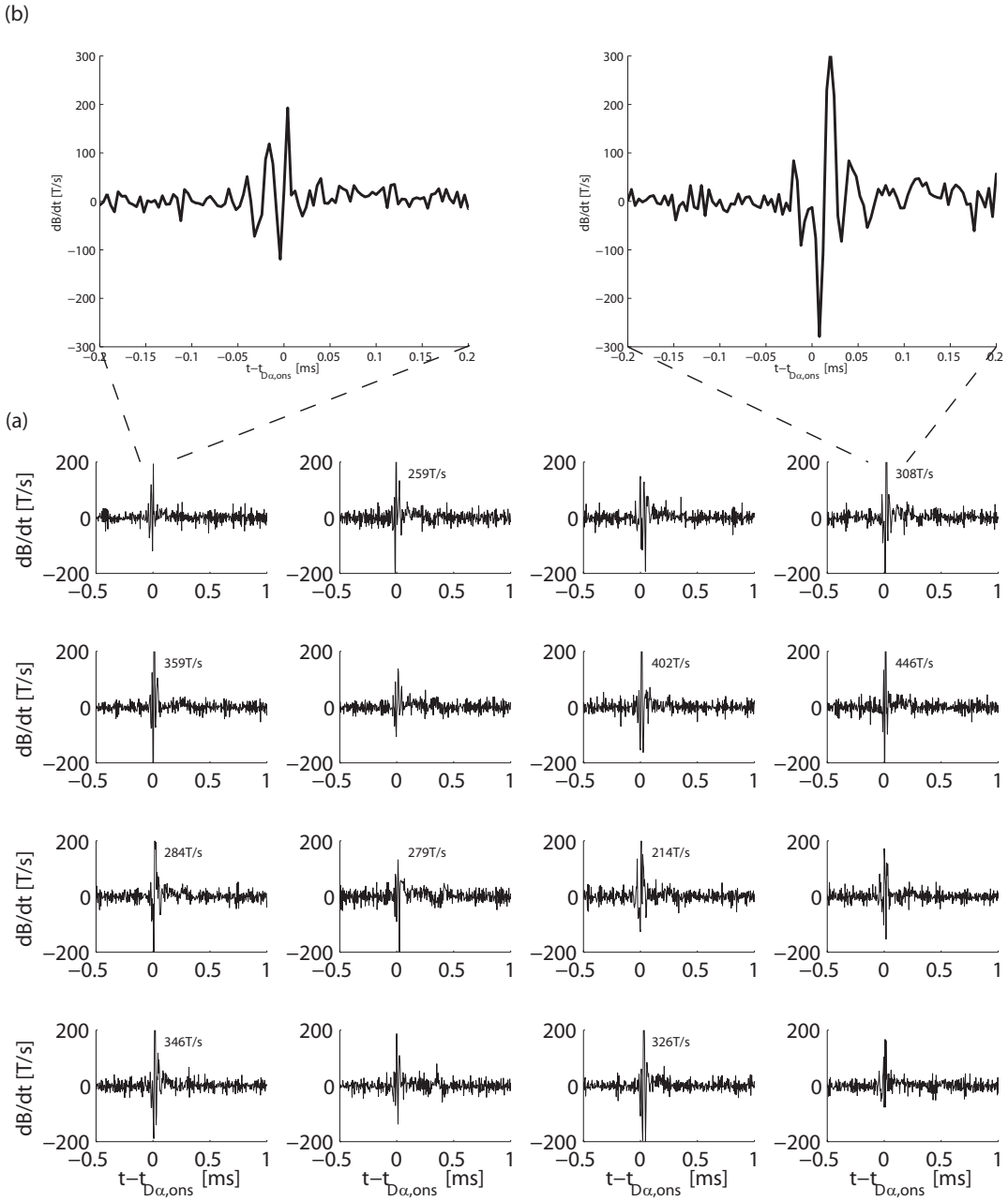

Figure 2. (a) Time derivative of the poloidal magnetic field acquired by a probe in the upper toroidal array for 16 subsequent ELMs in discharge 42062 (0.6s to 0.7s). The maximum absolute value is noted in the plots for cases, where it is exceeding the range displayed. (b) Close up for first and fourth ELM.

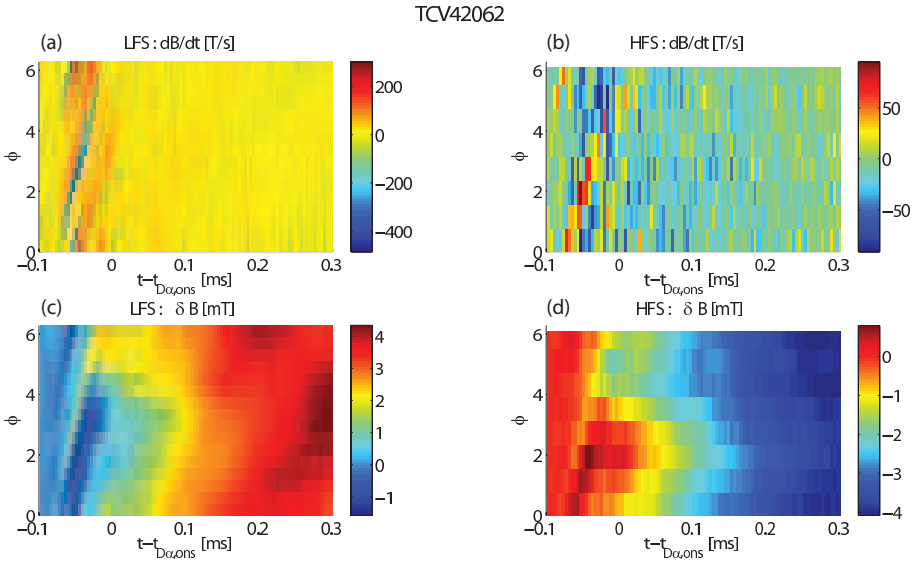

Figure 3. Magnetic perturbation during an ELM at 0.6107s in discharge 42062: dB/dt (upper row) and δB (lower row) for outboard side (left) and inboard side (right) as a function of time and toroidal position. δB is obtained from dB/dt by integration starting at a time corresponding to the left boundary of the displayed time interval.

trajectory of a local maximum (peak trajectory) of δB. Naturally a corresponding structure is observed on the plot of dB/dt on the outboard side.

For the inboard side due to the reduced number of probes per toroidal rotation the existence of peak or dip trajectories is less clear, but a trace of a peak trajectory can be identified (figure 3(d)). This is remarkable, as in a classical ballooning model the mode structure has negligible perturbation amplitude in this poloidal region.

3.2. Dynamics of dominant magnetic perturbations

The onset dynamics of dominant magnetic perturbations is of special interest. It may be compared to typical MHD time scales. The setup of the magnetic diagnostic in TCV enables the detailed study of the growth and decay of single dominant magnetic excursions. Figure 4(a) shows the evolution of the magnetic perturbation $\delta B(t, \phi)$ obtained by integration from a point in time before the ELM. The $n = 0$ component is subtracted for each time step. A dedicated algorithm identifies the trajectory $\phi_{\mathrm{traj}}(t)$ of a peak (dip) in δB. The white cross in figure 4(a) corresponds to the time and toroidal position of the absolute maximum (minimum) of δB over all probes and in a certain time window, which corresponds to the range displayed. Starting from this position alternately a step in time and the search for the local maximum (minimum) of δB as a function of ϕ is carried out (black crosses in figure 4(a)).

In figure 4(b) the evolution $\delta B_{\mathrm{traj}} = \delta B(t, \phi_{\mathrm{traj}}(t))$ of the magnetic perturbation on the identified trajectory is displayed. δB_{traj} rises from an inter-ELM value to the peak value within some tens of μs. After that it decays on a slightly slower time scale. The

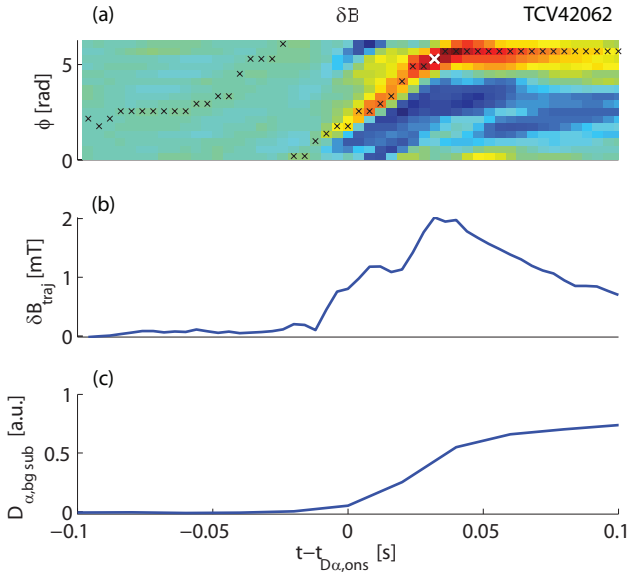

Figure 4. Peak trajectory of a magnetic perturbation during an ELM at 0.6107s in discharge 42062: (a) Evolution of δB obtained by integration starting at a time corresponding to the left boundary of the displayed time interval. The n=0 component is subtracted for each time step. White and black crosses mark the identified trajectory of the perturbation peak (algorithm described in the text). (b) δB on the peak trajectory (c) D_α-radiation from divertor and main chamber subtracted by the inter-ELM level.

D_α-radiation from divertor and main chamber (figure 4(c)) begins to increase close to the time, when δB_{traj} starts to clearly exceed the inter-ELM level. A growth rate is not extracted from figure 4(b), as the ELM is already in its non-linear phase when the inter-ELM fluctuation level is exceeded (subsection 3.4).

In order to identify the characteristics of the dynamics of δB_{traj} coherent averaging is used. The onset time $t_{\mathrm{D}\alpha,\mathrm{ons}}$ of D_α-radiation is used as a reference time for the temporal alignment (figure 5(a)). Figure 5(b) shows the coherent average of the evolution of δB_{traj}. The rise phase is shorter than 0.1ms, while the decay phase is a little longer.

3.3. Direction and velocity of dominant magnetic excursions

In order to analyze the propagation of magnetic perturbations, again the algorithm for the identification of peak (dip) trajectories is employed (section 3.2). Tracing the peak trajectory in figure 4(a) in time leads to a propagation in the positive toroidal direction. Considering the right-handed helicity of the field lines in discharge 42062, this can be mapped into the perpendicular direction, which corresponds to the electron diamagnetic drift direction. Hence the magnetic excursions propagate into the electron diamagnetic drift direction as in the majority of cases at ASDEX Upgrade investigated in [13].

Again in order to obtain more representative information the tracing algorithm is combined with coherent averaging. Figure 5(c) shows the coherent average of the toroidal position of the peak trajectory. The individual trajectories have been shifted to

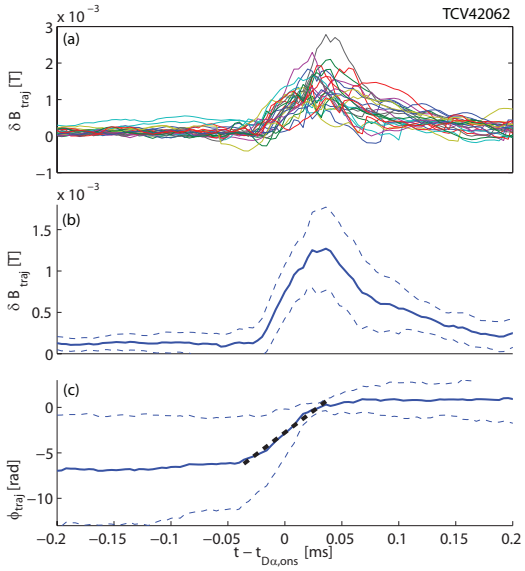

Figure 5. Identification of peak trajectories in combination with coherent averaging during ELMs in discharge 42062:(a) δB_{traj} evolution aligned using reference time $t_{\mathrm{D}\alpha,\mathrm{ons}}$ ($n = 0$ component subtracted for each time step). A quarter of the identified ELMs have been disregarded due to failure of the tracing algorithm. (b) Coherent average of δB_{traj} evolution (solid) with interval of width 2 standard deviations around (dashed). (c) Coherent average of the toroidal position of the peak trajectory (solid) with interval of width 2 standard deviations around (dashed). The individual trajectories have been shifted to $\phi = 0$ at the time of the maximum of the average δB_{traj} and unwrapped. The black dashed line shows the result of a linear fit during the phase of fastest propagation.

$\phi = 0$ at the time of the maximum of the average δB_{traj} and unwrapped. It is important to note, that with this aproach the significance of the quantity *averaged peak position* is higher, if δB_{traj} is high. The average apparent toroidal velocity is relatively low until about 50μs before $t_{\mathrm{D}\alpha,\mathrm{ons}}$. Around $t = t_{\mathrm{D}\alpha,\mathrm{ons}}$ it rises to relatively high values and falls to lower values about 50μs after $t_{\mathrm{D}\alpha,\mathrm{ons}}$. The time interval of high rotation velocities coincides with the rise phase of δB_{traj}. The linear fit for this phase, which is indicated in figure 5(c), corresponds to an average apparent toroidal velocity of 105km/s at the outboard mid plane separatrix position.

For the given time interval this velocity of the dominant magnetic excursion is compared to the electron diamagnetic drift velocity projected into the toroidal direction given by

$$v_{*e,\phi} = \frac{R}{e \cdot n} \frac{dp_e}{d\psi},$$

where n is the density and p_e is the electron pressure. A lower limit of the pressure gradient is calculated from the maximum difference of neighboring channels of the Thomson scattering diagnostic system in the plasma edge. The resulting value of $v_{*e,\phi}$ of 26km/s is clearly lower than the average of the apparent perpendicular velocity of the dominant excursions. The difference of these values has to be explained by the local

$E \times B$-velocity in combination with a possible phase velocity of the mode relative to the electron gas.

3.4. Toroidal profile and mode structure of dominant magnetic perturbations

The toroidal structure of magnetic perturbations during ELMs is a key feature to compare to linear and non-linear calculations. The magnetic diagnostic in TCV offers excellent conditions to investigate this structure.

The evolution of δB profiles during the phase δB_{traj} is rising to its highest value is investigated. Employing the algorithm identifying peak (dip) trajectories introduced above (section 3.2) the average apparent toroidal velocity of a dominant excursion is evaluated. The toroidal profiles are analyzed in the frame moving with this velocity, where the dominant excursion is at rest.‡ Figure 6(a) and (b) shows the evolution of a magnetic perturbation in $t-\phi$-space and the corresponding evolution of δB_{traj} during a phase, in which δB_{traj} is growing more than a factor of 10 up to its maximum value. Figure 6(c) shows the associated evolution of the shifted profiles normalized by δB_{traj}. In the early time instances the profiles are clearly influenced by background fluctuations. In particular the minimum at $\phi \approx \pi/2$ is evolving in relative depth. However a rigid fundamental shape is maintained throughout the entire time interval displayed. A similar behavior has been observed for the majority of ELMs. This observation documents that the temporal and the spatial dependence of the magnetic perturbation are approximately separable, allowing the magnetic perturbation to be described as:

$$\delta B(t,\phi) = g(t) f(\phi_R) \text{ ,where } \phi_R = \phi - \omega t$$

and ϕ_R is the toroidal angle in the system rotating with the perturbation, g is a function describing the overall growth and decay of the perturbation and f represents a rigid fundamental toroidal mode structure.

The observation of a rigid toroidal mode structure allows a further conclusion. Uncoupled mode components would usually rotate with different velocities and different radial mode component centers. Therefore the superimposed toroidal mode structure would evolve. Hence in the case reported here there is a strong indication of coupling of toroidal mode components. This in turn is an evidence that from exceeding the level of background fluctuations the perturbation has reached an amplitude, for which a linearization is not justified.

In order to investigate the fundamental toroidal structures of the perturbations the frame is chosen, in which the perturbation is at rest. After the toroidal shift the profiles

‡ Form the average apparent toroidal velocity a toroidal angle $\phi_{\mathrm{shift}}(t)$ is calculated, by which the profile at a given time has to be shifted, to be in the frame where the perturbation is at rest. To deal with the problem of discretisation of toroidal positions Fourier representation is chosen and the following identity is used: $FT(B(\phi+\phi_{\mathrm{shift}}(t),t)) = e^{i\phi_{\mathrm{shift}}(t)} FT(B(\phi,t))$, (*FT*:*Fourier transform*). From the obtained Fourier coefficients the shifted profiles in real space are reconstructed.

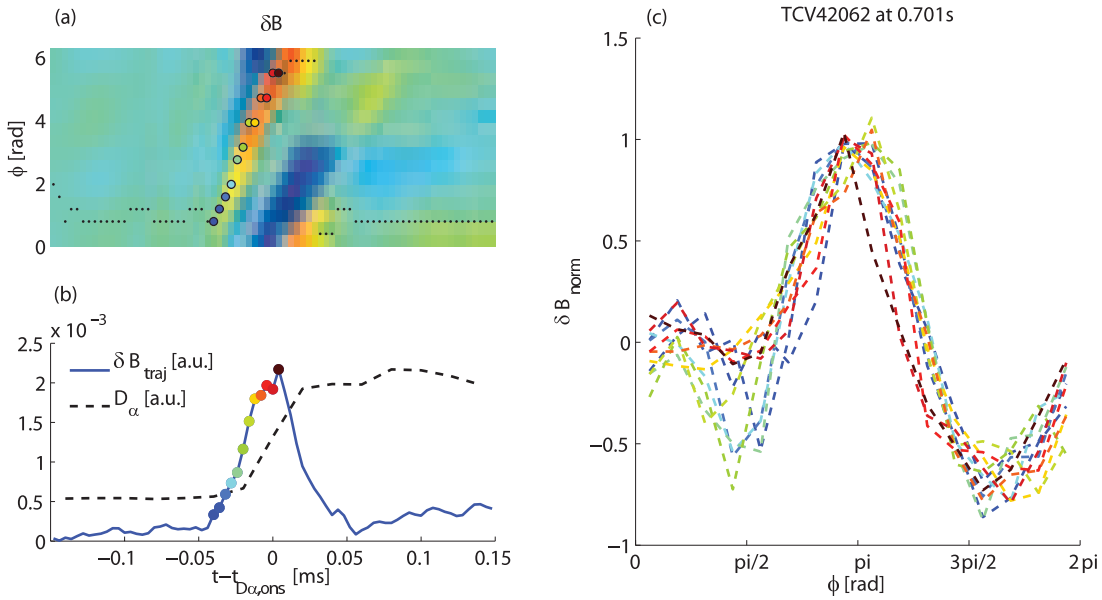

Figure 6. Evolution of profiles of δB in the rise phase of an ELM at 0.7011s in discharge 42062: (a) δB as function of t and ϕ. The identified trajectory is marked by dots (the larger ones in color indicate time steps shown in (b) and (c)). (b) Evolution of δB_{traj} and D_α-radiation. (c) Toroidal profiles of δB normalized by δB_{traj}(t). For the identification of time instances the same color code as for the dots in (a) and (b) is used.

are averaged for each toroidal position over time.§ The criteria for the selection of time instances t to include are:

1) $\delta B_{\mathrm{traj}}(t) > 0.5 \cdot \max(\delta B_{\mathrm{traj}})$,
2) the set of time instances is without gaps and ends at $t = t(\delta B_{\mathrm{traj}} = \max(\delta B_{\mathrm{traj}}))$.

Normalization to the overall growth (function g) is not applied, as the variation in amplitude is limited by the first selection criterion. More than 50% of the ELMs are deselected due to failure of the tracing algorithm or less than 4 time instances fulfilling the criteria. Figure 7 displays the shifted averaged profiles of δB for 8 ELMs in discharge 42062. A considerable range of profile shapes can be observed.

Even though the observed perturbations are a feature of the non-linear phase, it is instructive to analyze the corresponding amplitudes of the toroidal mode components. The sampling rate of 250kHz in combination with the rotation velocity allows for modes up to $n = 25$ to be resolved. The radial decay of magnetic perturbations depends on the local poloidal mode number, which is determined by the local field line inclination and the toroidal mode number. As the local field line inclination is rather constant close to the last closed flux surface (LCFS) at the outboard side it is straight forward to compensate this radial decay in the Fourier representation.

§ $FT(\sum_t B(\phi + \phi_{\mathrm{shift}}(t), t)) = \sum_t FT(B(\phi + \phi_{\mathrm{shift}}(t), t)) = \sum_t e^{i\phi_{\mathrm{shift}}(t)} \cdot FT(B(\phi, t))$

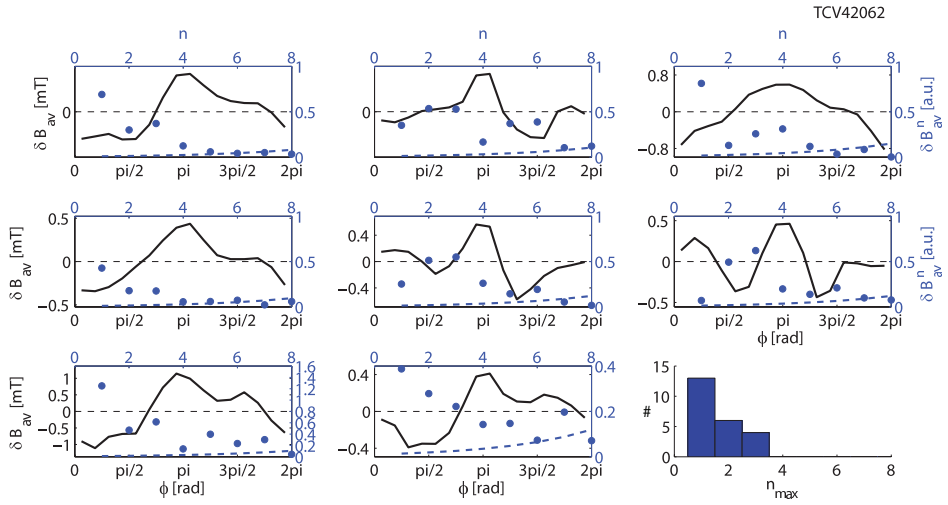

Figure 7. Shifted and averaged toroidal profiles of δB during the growth phase of 8 ELMs in discharge 42062: All figures except the bottom right one show for an individual ELM the magnetic perturbation δB_{av} averaged over a number of selected time instances as a function of ϕ (black). In the same plots the amplitudes of the mode components δB^n_{av} (compensated by $(r/r_P)^{0.91n}$) are illustrated (right and top axis, blue). The blue dashed lines represent the Fourier transform of the inter-ELM fluctuation level. The bottom right plot shows the histogram of the mode number $n_{\max}$ corresponding to the maximum amplitude of the mode component (radial decay effect compensated) over a set of 23 ELMs.

In order to assess this radial decay as a function of toroidal mode numbers a code has been used that is evaluating synthetic probe signals caused by a mode, which is represented as a superposition of current filaments [14]. For toroidal mode numbers $n = 1 - 8$ perturbations with identical amplitude in current density are simulated. Figure 8 illustrates the amplitude of the magnetic field component as measured by the probe as a function of toroidal mode number. In a basic cylindrical model with a single poloidal mode number m the radial decay of the magnetic field perturbations is proportional to $(r/r_P)^{-(m+1)}$, where r_P is the plasma radius. Transferring this to toroidal geometry one has to use the local poloidal mode number yielding as radial decay

$$(r/r_P)^{-(m_{\rm loc}+1)} = (r/r_P)^{-(d\phi/d\theta \cdot n+1)}.$$

The field line inclination $d\phi/d\theta$ locally at the outboard mid plane takes values of unity or even below. On the basis of these considerations the function $a \cdot (r/r_P)^{-b \cdot n}$ is fitted to the amplitudes in figure 8. For r/r_P the value 1.4 is used, which is the ratio of the minor radii of probe and LCFS in the poloidal position of the probe.

The general trend in figure 7 (circles - right and top axis) is that even with compensation of the radial decay effect described above the absolute values of toroidal mode component amplitudes δB^n_{av} are higher for low toroidal mode numbers than for high toroidal mode numbers. This can be expressed also in another way by counting the number of ELMs, for which $n = 1, 2, 3, ...$ is the mode number with the highest δB^n_{av}

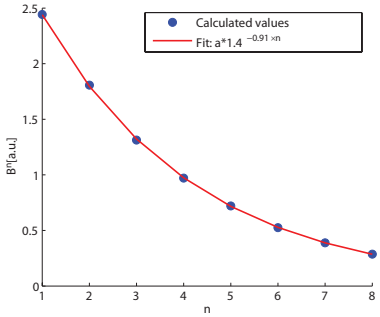

Figure 8. Mode number dependent radial decay of perturbations from a model constructing the mode from current filaments: The amplitude of the magnetic field component seen by the probe as a function of toroidal mode number for n=1,2,...,8 is shown as blue dots. The result of a fit ($|FC| = a \cdot 1.4^{-0.91 \cdot n}$) is shown as a red line.

(figure 7 bottom right plot). For a large majority of ELMs $n = 1$ is dominant.

It is important to assess, whether the Fourier components before the compensation are above the noise level. Therefore the Fourier transform of the inter-ELM fluctuation level is indicated as a dashed line in figure 7. Here it is assumed that these fluctuations are distributed uniformly to mode numbers $n = 1, 2, ..., 8$. Only in some cases the absolute value of the coefficients corresponding to the higher toroidal mode numbers are below this level. However this casts no doubt on the general trend of components with low toroidal mode number dominating.

It is further analyzed, if the dominance of the low toroidal mode numbers is just the result of aliasing. For a system with 16 equally spaced probes $n = 8$ is the spatial correspondence of the Nyquist frequency. First, in a basic model ($\delta B(\phi, t) = B_0 \sin(n\phi - \omega t)$) the apparent angular velocity $v_{\mathrm{peak},\phi}$ of the peak in real space is compared to the time derivatives $d/dt(\arg(a_n))$ of the angle of the Fourier coefficients. For $0 < n < 8$ the signs of $v_{\mathrm{peak},\phi}$ and $d/dt(\arg(a_n))$ are opposite, while they are identical for $8 < n < 16$. This can be explained by an aliasing effect in the latter case. Figure 9 shows the evolution of δB for an ELM at 0.6533s in discharge 42062. Also the evolution of the phase angles of the Fourier coefficients ($n = 1 - 8$) are illustrated for time instances, at which δB^n_{av} is exceeding 10% of the maximum over the time interval displayed and over toroidal mode numbers 1 to 8. The signs of $v_{\mathrm{peak},\phi}$ and $d/dt(\arg(a_n))$ are opposite. This is a clear indication that the mode components for $0 < n < 8$ are stronger as the ones for $8 < n < 16$ and that aliasing is playing no or only a minor role.

The finding, that the $n = 1$ component is most often dominant, is now compared to results from linear stability calculations with the code KINX [15] presented in [16]. KINX evaluates the linear growth rates of coupled peeling-ballooning modes. As input information the geometry of the plasma boundary and profiles of pressure and current density are used. KINX generates a stability map in normalized pressure gradient α and parallel current density.

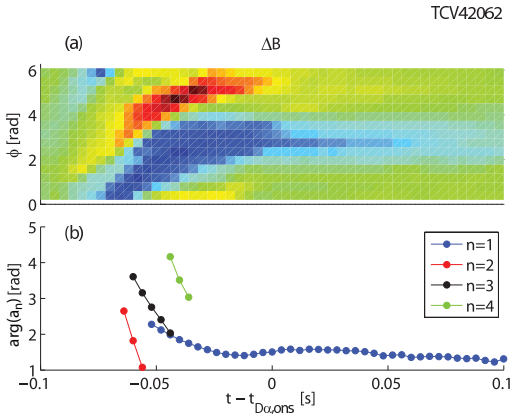

Figure 9. Comparison of velocities for an ELM at 0.6533s in discharge 42062: (a) δB as function of ϕ and t (b) Phase of the Fourier coefficients for $n = 1 - 4$. Only time instances are displayed at which the absolute value of the Fourier coefficient is exceeding 10% of the maximum over the time interval displayed and toroidal mode numbers 1 to 8.

Some of the calculations presented in [16] are based on experimental data from discharge 38008, which has similar values as 42062 for toroidal magnetic field, plasma current and electron density and temperature at the pedestal top. The discharges differ in total heating power (38008: 0.9MW, 42062: 1.5MW) and the position of the outer strike point (38008: bottom wall, 42062: outside wall). In both discharges ELMs are identified as type-I.

For parameters corresponding to 38008 and a time just before the ELM crash KINX finds the first unstable mode to have a toroidal mode number of 15 or larger. Also in other linear stability calculations the most unstable toroidal mode number is clearly larger than n=1 [17]. In summary the dominant toroidal mode numbers observed in the experiment ($n \in \{1, 2, 3\}$) strongly differ from the first linearly unstable toroidal mode numbers in linear stability calculations.

4. Summary and discussion

The analysis reported in this publication concentrates on magnetic perturbations during type I ELMs in TCV. Enhanced magnetic activity associated with ELMs in TCV is confined to dominant magnetic perturbations lasting up to about 0.15ms around the onset of D_α-radiation from main plasma and divertor. These dominant magnetic excursions propagate in the electron diamagnetic drift direction. For the investigated time interval an average apparent toroidal velocity of about 100km/s has been calculated.

The growth of dominant magnetic perturbations from their detection until reaching the peak perturbation level lasts less than 0.1ms. The toroidal shapes at all time instance during this phase are similar to each other (rigid mode-structure). This can only be explained by non-linear coupling of toroidal mode components. Hence magnetic

perturbations during the linear ELM phase cannot be observed by magnetics in TCV.

Most frequently the strongest toroidal mode component of dominant magnetic perturbations is found to be $n = 1$. In the corresponding analysis the radial decay of perturbations, which depends on the local poloidal mode number, has been compensated in a way that the mode components at the LCFS position are compared. As a dominant aliasing effect has been excluded the statement is valid for the range $1 \leq n \leq 15$.

In comparison to this result investigations by Thomson scattering [18] at ASDEX Upgrade have been extrapolated to 10 to 20 blobs per toroidal rotation. Also measurements from divertor infrared thermography [19] show 8 to 20 peaks per toroidal rotation. However, as both of these techniques are based on the toroidal distance of neighboring peaks, they are not suitable to capture components associated with the lowest toroidal mode numbers, even if these are dominant. Hence the ASDEX Upgrade results do not contradict the dominance of the $n = 1$ component in dominant magnetic perturbations found in this work.

The key result that at TCV in the non-linear phase the dominant toroidal mode number of dominant magnetic perturbations is most frequently n=1 is put in context with a KINX calculation. This linear stability calculation for another but comparable TCV discharge shows that the most unstable modes at the operational point have mode numbers $n > 15$. In combination this suggest that from the linear to the non-linear phase the dominant toroidal mode number changes from intermediate ($n \gtrapprox 15$) to low values ($n \approx 1$) values. This is consistent with recent results from non-linear simulations with the code JOREK [20].

The evolution of toroidal mode numbers might explain the relatively large losses of energy routinely observed during type I ELMs. Linear calculations clearly show that modes with low toroidal mode numbers are more global. They extend more towards the plasma center than modes with higher toroidal mode numbers.‡ If there is also such a structural difference in a non-linear situation, the low n components could lead to erosion of temperature and density from areas further inside.

5. References

[1] Connor J W 1998 *Plas.Phys.Contr.Fusion* **40** 191–213
[2] Snyder P B, Wilson H R, and Xu X Q 2005 *Physics of Plasmas* **12** 056115
[3] Coda for the TCV team S 2011 *Nuclear Fusion* **51** 094017
[4] Rossel J *et al* 2012 *Nuclear Fusion* **52** 032004
[5] Moret J M, Buhlmann F, Fasel D, Hofmann F, and Tonetti G 1998 *Review of Scientific Instruments* **69** 2333–2348
[6] Valovic M *et al* 1994 *21th EPS Conference on Controlled Fusion and Plasma Physics*
[7] Becoulet M *et al* 2003 *Plasma Physics and Controlled Fusion* **45** A93–A113
[8] Bobkov V *et al* 2004 *31th EPS Conference on Controlled Fusion and Plasma Physics*
[9] Neuhauser J *et al* 2008 *Nuclear Fusion* **48** 045005
[10] Sommer F *et al* 2011 *Plasma Physics and Controlled Fusion* **53** 085012

‡ Low n modes also have a larger poloidal extension compared to high n modes.

[11] Koslowski H *et al* 2005 *Nuclear Fusion* **45** 201–208
[12] Solano E R *et al* 2010 *Physical Review Letters* **104** 185003
[13] Wenninger R *et al* 2012 *Nuclear Fusion* **52** 114025
[14] Reimerdes H, Sauter O, Goodman T, and Pochelon A Feb 2002 *Phys. Rev. Lett.* **88** 105005
[15] Degtyarev L *et al* 1997 *Computer Physics Communications* **103** 10 – 27
[16] Pitzschke A *et al* 2012 *Plasma Physics and Controlled Fusion* **54** 015007
[17] Snyder P *et al* 2009 *Nuclear Fusion* **49** 085035
[18] Kurzan B *et al* 2005 *Physical Review Letters* **95** 145001
[19] Eich T *et al* 2003 *Physical Review Letters* **91** 195003
[20] Krebs I, Hoelzl M, Lackner K, and Guenter S 2013 *Physics of Plasmas - submitted*